Plasma Chemistry and Plasma Processing
https://doi.org/10.1007/s11090-022-10233-7

ORIGINAL PAPER

Quantitative Schlieren Diagnostics Applied to a Millisecond Pulsed-DC Hybrid Discharge in Atmospheric Pressure Air

E. Cejas[1] · **J. C. Chamorro**[1] · **L. Prevosto**[1,2]

Received: 18 October 2021 / Accepted: 27 January 2022

Abstract
The gas temperature of a hybrid discharge in atmospheric pressure air is investigated by using quantitative schlieren imaging. The discharge is stabilized in a pin-to-plate electrode geometry and operated in a millisecond pulsed-DC regime with current amplitudes up to 75 mA and a duration of 10 ms, applied at a frequency of 100 Hz. An equilibrium composition model is considered to account for the production of N, O, and NO, which influence the Gladstone–Dale coefficient of air at high-gas temperatures. Also, a procedure is described which allows the determination of the errors introduced in the time-average gas refraction index due to gas temperature fluctuations. The results show that the axial values of the gas temperature profiles span a large range from ~ 1000 to 5000 K, nearly following the evolution of the discharge current. The temperature values found agree well with those reported in the literature for atmospheric pressure air plasmas, ranging from micro-glow to hybrid discharges.

Keywords Hybrid discharge · Schlieren technique · Gas temperature · Fluctuations

Introduction

Atmospheric pressure non-equilibrium (or non-thermal) plasmas have attracted much attention since the nineteenth century, owing their unique aspects as compared to their low-pressure counterparts [1]. So far atmospheric pressure non-equilibrium plasmas have been studied for a wide field of technological applications through a variety of plasma generation mechanisms [2]. In particular, atmospheric pressure glow-type discharges were intensively studied in the last decade, both in the low-current regime (~ 1–10 mA, see e.g., [3–5]) as well as in the intermediate-current regime (~ 50–400 mA, see e.g., [6–8]). The intermediate-current glow discharge is always contracted, with a rather high-gas temperature, but

✉ E. Cejas
cejasezequiel87@gmail.com

[1] Grupo de Descargas Eléctricas, Depto. Ing. Electromecánica, Facultad Regional Venado Tuerto, Laprida 651, Venado Tuerto (2600), Santa Fe, Argentina

[2] CONICET, Facultad Regional Venado Tuerto Departamento Ing. Electromecánica, Grupo de Descargas Eléctricas, Universidad Tecnológica Nacional, Laprida 651, Venado Tuerto (2600), Santa Fe, Argentina

Published online: 18 February 2022

the thermal non-equilibrium state is still maintained at a high-level. It can be regarded as a hybrid (or filament) [9] discharge, lying between the diffusive glow discharge and the thermal arc [6]. However, because of its contracted properties, the thermal state of such discharges is difficult to investigate experimentally and is not yet well characterized. Optical emission spectroscopy (OES) methods are commonly applied to measuring plasma temperatures [4, 5], although these methods are often restricted by the distribution of corresponding excited species. Another optical method used to measure gas temperature is the Rayleigh scatter thermometry (RST) [7]. This method has the advantage over OES-based methods that it allows the observation of the entire state representation of gas particles within the discharge (not just an excited state), but it is only accurate up to gas temperatures about 2000 K [10].

The schlieren diagnostic has been extensively used for centuries to investigate phenomena occurring in transparent media, mainly providing qualitative information [11]. Nowadays, a number of works have been devoted to obtaining fundamental quantitative knowledge in a variety of geometries and applications of atmospheric pressure plasma sources; ranging from micro-plasma jets to thermal plasma torches (e.g., see the recent review in [12] and references therein; see also the works in [13] and [14]). More recently, also quantitative schlieren diagnostics were applied to measure the gas temperature in a DC glow discharge in the low-current regime (6–16 mA) [15]. However, despite the great interest and importance of the intermediate-current glow discharges owing to their high-power density, at present there are no quantitative schlieren studies of hybrid discharges. The development of such a study is the main purpose of this paper.

In this paper, the schlieren diagnostic is used to quantitatively study the thermal state of a millisecond pulsed-DC, pin-to-plate hybrid discharge in atmospheric pressure air. The discharge is operated with current pulses up to 75 mA and a duration of 10 ms, applied at a frequency of 100 Hz. Factors such as fluctuations in the discharge current, and the validity of assumptions often used for the calculation of the gas refraction index in non-thermal plasmas are considered. The obtained results are compared with the available data and good agreement is found.

Experimental Setup and Techniques

Hybrid Discharge

The electrical circuit used to generate and stabilize the millisecond pulsed-DC hybrid discharge in atmospheric pressure air is similar to that used in [6], but the electrodes configuration was changed in order to improve the stability and symmetry of the discharge. The discharge is generated between two copper electrodes (20 mm in diameter) with the cathode having a sharp tip and the anode a flat surface, aligned in a vertical pin-to-plate configuration, with the anode above the grounded cathode. The gap length between electrodes is fixed to 1 mm. With this electrode configuration, a spatially stable discharge with minimal deviations from the cylindrical symmetry is generated. In order to remove any oxide layer on the electrode surfaces that can cause some temporary transitions to the arc phase, the electrodes are polished with a fine grade emery paper and then cleaned. Several repeatable and consistent measurements were obtained after re-polishing and cleaning the electrode surfaces [6, 16].

The AC power supply is a high-voltage transformer operating at low frequency (50 Hz) with a high-dispersion reactance connected to a variable autotransformer to control the discharge current. The output of the transformer is connected to a semiconductor full-wave rectifier. Because of the high-impedance of the transformer provides an intrinsic current limitation, the use of external ballasts is not necessary to stabilizes the discharge. The discharge current is measured using a (low-inductance) shunt resistor of 100 Ω, while the discharge voltage is measured by employing a resistive-capacitive voltage divider (Tektronix P6015A, 1000X, 3pf, 100 MΩ). Both electrical signals are simultaneously registered by using a 4-channel oscilloscope (Tektronix TDS 2004C with a sampling rate of 1 GS/s and an analogical bandwidth of 70 MHz).

The discharge current together with the discharge voltage are shown in Fig. 1. The discharge is ignited by a streamer-to-spark, high-voltage transition (voltage spikes up to 8 kV are found at the beginning of each pulse), but soon after the breakdown the voltage drops to several hundred volts (~400 V) due to the high-impedance of the transformer, and the hybrid discharge stabilizes. Some current spikes appear also at the beginning of each pulse, correspond to unsuccessful electric breakdowns interrupted by the fast current limitation. The measured cathode fall (~360 V) [6] is typical for air glow discharges with Cu cathodes [9]. The stable operation of this discharge is supposedly provided by the secondary electron emission from the cathode. The discharge current pulses with a main frequency of 100 Hz at an amplitude of 75 mA limited by the transformer impedance. The voltage waveform also pulses with a frequency of 100 Hz and decreases when the current increases, thus, leading to a negative slope in the voltage–current characteristic of the discharge –inset of Fig. 1 b)–.

The discharge operating power is calculated by averaging the product of the current and voltage waveforms to be 28 W. As the calculated discharge power already includes the electrode voltage falls, only a fraction of that discharge power goes to gas heating in the plasma column. An important remaining part is dissipated by thermal conduction and several excitation processes in the electrode sheaths (mainly the cathode) [9].

Optical System

Figure 2 shows a schematic of the *Z*-type [11] schlieren setup used in the experiments. A red LED (main light wavelength at $\lambda = 630$ nm) with a 632.8 nm (± 4.4 nm FWHM) band-pass filter is used to generate a monochromatic light background. To homogenize

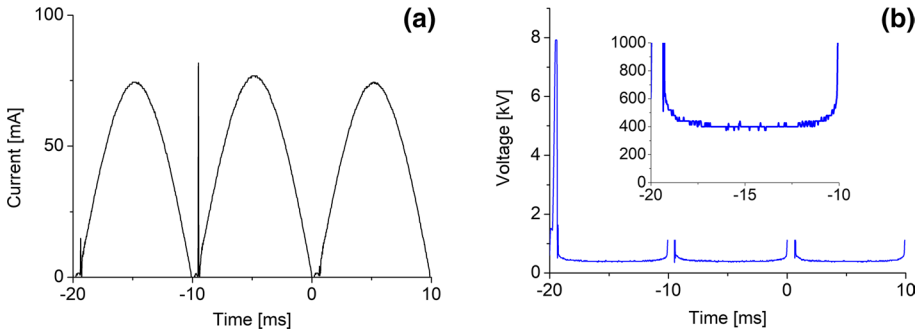

Fig. 1 Typical discharge (**a**), and voltage (**b**), waveforms of the discharge

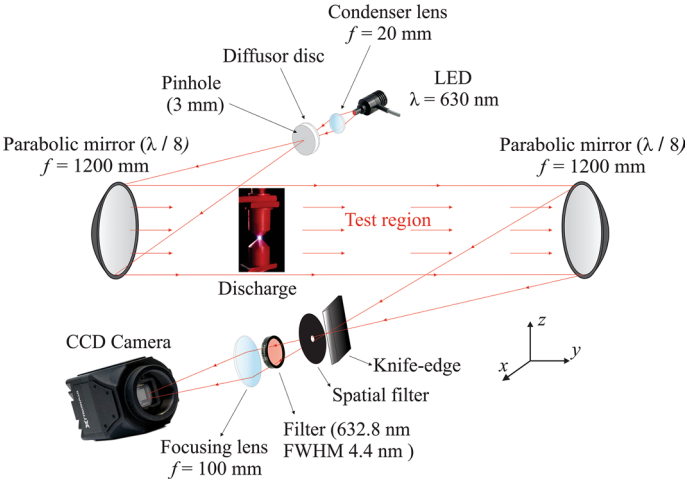

Fig. 2 Schematic of the schlieren *Z*-type optical set-up

the light background a condenser lens (focal length, $f = 20$ mm) with a diffuser disc and two parabolic mirrors ($f = 1200$ mm, $\lambda/8$) are used. A knife-edge is placed at the focus of the focusing parabolic mirror to provide the best sensibility perpendicular to the discharge axis. The position of the knife edge is adjusted so that the detected intensity signal was approximately 48% of the signal intensity without the presence of the knife-edge. A spatial-filter is also set at the focus of the focusing mirror to reduce the influence of the plasma brightness in the schlieren images [17]. The final schlieren image size is controlled independently with a focusing lens ($f = 100$ mm). The optical setup is carefully aligned to minimize off-axis errors. The schlieren images (with a resolution of 2048×1088 pixels) are captured with a CCD camera (Lumenera Lt225M) with variable exposure time (1/2000 and 1/10 s). The images are stored in BMP format and digitized by an 8–bit gray-level frame grabber. According to the magnification of the optical system employed, the spatial resolution of the schlieren image is ~ 0.03 mm. The schlieren system is calibrated by using a 'weak' lens according to the method described in [18] and recently used in [15, 19]. The transverse refractive angle ε_x in the schlieren image of the discharge is quantified by using the calibration $f = 10$ m focal-length lens according to,

$$\varepsilon_x = \frac{1}{f}(r - r_0), \tag{1}$$

where r and r_0 are the radial positions in the calibration lens (measured along the horizontal diameter from the lens center) with same schlieren signal contrast $C(x)$ to that of the transverse x-position in the discharge region, and the zero-contrast value (background without disturbance), respectively [18]. The contrast is defined as the ratio of the differential intensity at a given image pixel to the value of its background level intensity [11]. The contrast gradient within the lens image is observed as a purely horizontal gradient because a vertical knife-edge cutoff is used (Fig. 2). During the experiment the discharge and calibration lens are photographed separately, by setting them in the same plane of field. The result of this procedure is shown in Fig. 3 (the measuring contrast range is indicating by dashed lines in Fig. 3). It is observed that the schlieren system operates in the linear region.

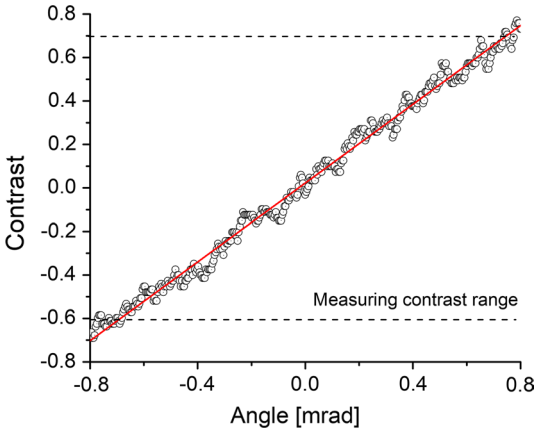

Fig. 3 Calibration curve (Color figure online)

The corresponding sensitivity is calculated from the slope of the calibration curve (indicated with a red line in Fig. 3) to be $S = 933$.

One critical aspect of this calibration procedure is that each point within the calibration lens image has a unique contrast value and that corresponding contrast values are also observed in the schlieren image. The contrast range observable in the calibration lens represents the measuring range of the schlieren system (i.e., the range of light refraction angles that are observable). This range of observable refractions must be balanced with the sensitivity of the schlieren system (i.e., the minimum refraction angle that can be detected) in order to achieve the full spatial–field visualization of gas temperature in the discharge.

Schlieren Theory

Mathematical details of the schlieren diagnostic are available from many sources (e.g., [11, 20]). In transparent and inhomogeneous media, light rays suffer deviations that are related to the local refractive-index gradient and the extent of the light-ray-path in the medium under study (i.e., the schlieren imaging is integrative). In the present conditions these deviations occur in the transverse x-direction (see Fig. 2). Provided that: (i) the measuring range of the schlieren system has not been exceeded, (ii) the schlieren system operates in the linear region, and (iii) the transparent medium has axisymmetric properties; it can be shown that the contrast C measured on the image relates to the refractive index in the test region as:

$$C(x) = 2x\frac{S}{n_\infty}\int_x^\infty \frac{\partial n}{\partial r}\frac{dr}{\sqrt{r^2 - x^2}}, \tag{2}$$

where n is the gas refraction index ($= n_\infty$ where the contrast vanishes) and r the radial position measured from the discharge axis. $n(r)$ is obtained from the modified Abel inverse integral of (2), given as,

$$n(r) = n_\infty - \frac{1}{\pi}\frac{n_\infty}{S}\int_x^\infty \frac{C(x)}{\sqrt{r^2 - x^2}}dx. \tag{3}$$

Equation (3) is used with experimental data $C(x)$. Note that differentiation of the experimental data is not required. This becomes one of the main advantages of the schlieren technique over interferometry.

The precise determination of the gas temperature (T) of the discharge requires the knowledge of the plasma composition. In non-equilibrium plasmas in air and other gases, the Gladstone–Dale coefficient of the gas is usually regarded as a material constant equal to its room temperature value (see e.g., [15]). This means that the chemical composition of the gas does not vary with increasing temperature (i.e., 'frozen chemistry'). However, chemical processes like dissociation phenomena influence the Gladstone–Dale coefficient which is higher for O_2 than for O (by a factor of 1.06) and smaller for N_2 than N (by a factor of 0.79). In order to account for the error introduced by such simplification under rather high-gas temperature conditions, the gas composition is obtained by a simple model. Since the degree of ionization is very low under the present conditions, the atomic species N, O, and NO are produced mainly by collisions among heavy species, so that, the numerical densities [N], [O], and [NO] are determined from the equilibrium constants at the gas temperature [6, 21],

$$\frac{[\mathrm{N}][\mathrm{O}]}{[\mathrm{NO}]} = 9.2\times10^{30}T^{1/2}\left[1-\exp\left(-\frac{E_{NO}}{T}\right)\right]\times\exp\left(-\frac{D_{NO}}{T}\right), \tag{4}$$

$$\frac{[\mathrm{N}][\mathrm{N}]}{[\mathrm{N_2}]} = 3.6\times10^{31}T^{1/2}\left[1-\exp\left(-\frac{E_{N_2}}{T}\right)\right]\times\exp\left(-\frac{D_{N_2}}{T}\right), \tag{5}$$

$$\frac{[\mathrm{O}][\mathrm{O}]}{[\mathrm{O_2}]} = 4.5\times10^{31}T^{1/2}\left[1-\exp\left(-\frac{E_{O_2}}{T}\right)\right]\times\exp\left(-\frac{D_{O_2}}{T}\right), \tag{6}$$

where T is in electronvolt. $E_{\mathrm{NO}}=0.23$, $E_{N_2}=0.29$ and $E_{O_2}=0.20$ are the vibrational quanta of NO, N_2 and O_2, respectively (in electronvolt); $D_{NO}=6.5$, $D_{N_2}=9.8$ and $D_{O_2}=5.1$ are the dissociation potential of NO, N_2 and O_2, respectively (in electronvolt). The numerical density of the dominant species N_2 is obtained from the constancy of the pressure ($p=$ one atmosphere), while the density of O_2 is determined according to the conservation of nuclei (N_2:$O_2\equiv 4$:1). It should be noted that the vibrational non-equilibrium facilitates the thermal dissociation of the nitrogen [22]. However, as a marked vibrational non-equilibrium of nitrogen molecules is only expected at low-gas temperatures values (i.e., at discharge currents typically <10 mA in air discharges, see e.g., [23]) in which the constant rate of thermal dissociation of nitrogen is very small; appreciable errors in the calculated gas composition are not expected. Also note that the optical refractivity of free electrons has been neglected. This is because the influence of free electrons becomes important only at ionization degrees of a few percent [20]. With the obtained gas chemical composition (shown in Fig. 4), the gas refraction index is then calculated according to the Gladstone–Dale relation under the ideal gas approximation [11, 20]:

$$n(T)-1=\frac{T_r}{T}\sum_i x_i(n-1)_{i,r}, \tag{7}$$

where $(n-1)_{i,r}$ and x_i are the reference refractivity and molar fraction for species i, (N_2, O_2, N, O, NO) respectively. The background gas temperature was measured to be $T_r=290$ K. Optical refractivities for N_2, O_2, and NO at 589.3 nm are taken from [20], and for O and

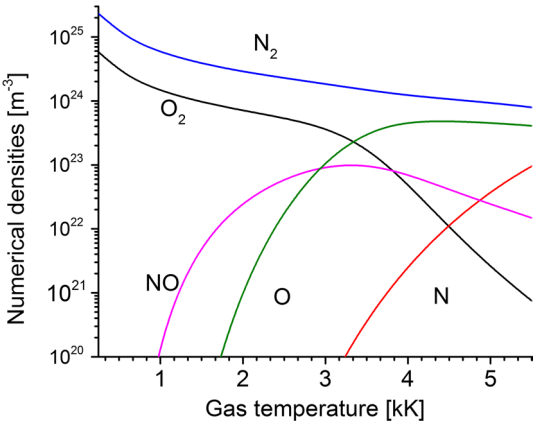

Fig. 4 Equilibrium air gas composition

N at 544.6 nm are taken from [24]. Both the gas refraction index for the frozen chemistry and that for the calculated chemistry composition, are shown in Fig. 5. It is seen that the simplification of using the room temperature Gladstone–Dale coefficient to calculate the index of refraction is justified in air up to gas temperatures about 5000 K. These estimates are consistent with results of optical interferometric experiments involving air at high-gas temperature [24]. It should be noted that under non-equilibrium conditions, in particular at low gas temperature values ($T < 3000$–4000 K), some underestimation is expected in the equilibrium densities shown in Fig. 4, because the atoms are also produced via electron-impact dissociation and the NO density is also affected by collisions with electronically excited particles produced by electron impact. However, in weakly ionized atmospheric pressure plasmas in air and other molecular gases, the electron mean energy is not so high, and the non-equilibrium gas composition is close to that of equilibrium (e.g., [21]). In any case, at relatively low gas temperatures, the densities of neutral species of the air other than O_2 and N_2 molecules can be ignored, and the resulting error in evaluating the refractive index of air is negligible.

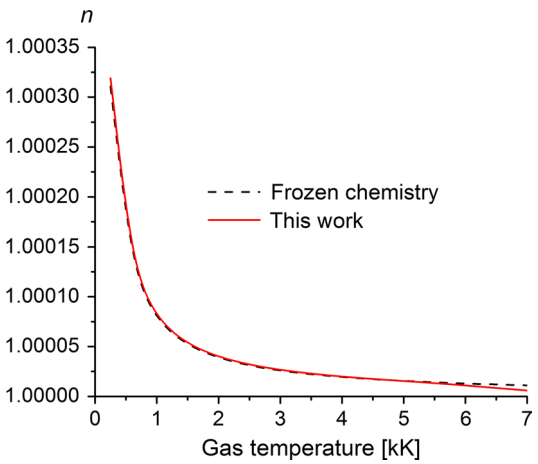

Fig. 5 Gas refraction index from both the frozen chemistry and the calculated equilibrium composition shown in Fig. 4

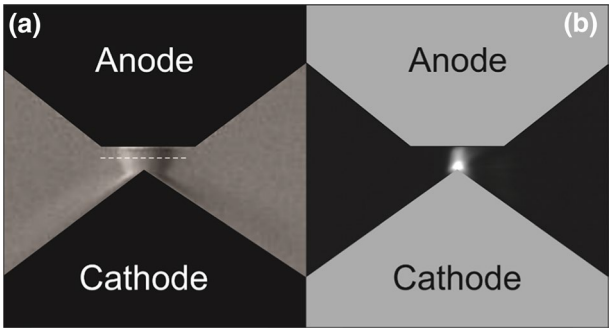

Fig. 6 Schlieren image of the discharge (**a**), and corresponding visible image (**b**)

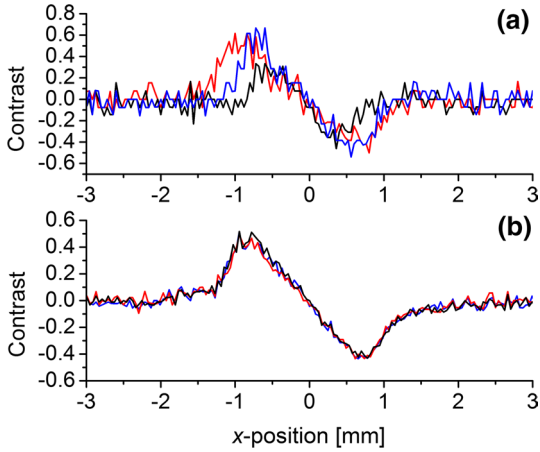

Fig. 7 Contrast profiles from several consecutive measurements at 1/2000s (**a**), and 1/10 s (**b**), exposure time

Results and Discussion

Data Processing

Figure 6a shows the time-averaged contrast pattern of the discharge obtained from an image with and exposure time of 1/10 s. Figure 6b shows the corresponding visible image. The spatial-resolutions and scales of discharge and schlieren images are the same. The visible emissive structure of the discharge resembles to that of a typical low-pressure glow, thus suggesting a similar electric field distribution in the discharge. By comparing the patterns of discharge luminance and schlieren, it is evident that the discharge luminous region is much narrower than that of the corresponding schlieren image due to the contracted plasma channel of the discharge.

The measured radial contrast profiles along the line shown in Fig. 6 are shown in Fig. 7. Figure 7a shows three consecutive measurements taken with a short exposure time of 1/2000s and Fig. 7b shows consecutive measurements taken with an exposure time of 1/10 s. There are large differences between the contrast profiles in the discharge zone when the short exposure time is used, that are masked by time-integration with longer exposure time. These differences are mainly attributed to large fluctuations in gas temperature caused by the discharge current waveform (with a main timescale of 1/100 s). Note that there is also a certain level of fluctuation (noise) in the background that is not associated

with the discharge itself. Despite the presence of some noise level, the measured contrast profiles given in Fig. 7 demonstrate that the studied pin-to-plate discharge is spatially stable and fairly symmetric.

Plasma Fluctuations Analysis

Plasma fluctuations are an important feature of gas discharges (see e.g., [25]). They can influence the calculation of the plasma properties by introducing errors in the experimental data if measurements are made on timescales larger than those of fluctuations. Errors introduced in plasma fluctuating scenarios have already been addressed in OES measurements (see, e.g., [26]) as well as in electrostatic probe measurements (see, e.g., [27]), but not in schlieren measurements.

In particular, in an oscillating scenario, the average gas refraction index is not easily related to the gas refraction index at the gas average temperature. If a fluctuating gas temperature is taking into account in the gas refraction index, it can be expressed as,

$$\langle n\rangle + n' = n\big(\langle T\rangle + T'\big), \tag{8}$$

where $\langle\rangle$ indicates the time-average part and comma indicates the fluctuating part (with zero-time average). Equation (8) can be expanded around $\langle T\rangle$ to give,

$$\langle n\rangle + n' = n(\langle T\rangle) + \frac{dn}{dT}T' + \frac{1}{2}\frac{d^2n}{dT^2}T'^2 + \frac{1}{6}\frac{d^3n}{dT^3}T'^3 + \frac{1}{24}\frac{d^4n}{dT^4}T'^4 + \ldots, \tag{9}$$

where all the refraction index derivatives are evaluated at the averaged value of the gas temperature. Taking the time-average of (9),

$$\langle n\rangle = n(\langle T\rangle) + \sum_m \frac{1}{m!}\frac{d^m n}{dT^m}\langle T'^m\rangle. \tag{10}$$

It is seen from (10) that there is an additional refraction index term related to the presence of a fluctuating gas temperature. The terms $\langle T^m\rangle$ with $m>2$ in (10) cannot be reduced in terms of the gas temperature variance $\langle T^2\rangle$ and are not available experimentally either. However, it is certainly reasonable to approximate these by assuming that T' follows a sine wave (i.e., $\langle T^4\rangle = 1.5\langle T^2\rangle^2; \langle T^6\rangle = 2.5\langle T^2\rangle^3$, etc.) [26, 28]. Then, (10) contains only two dependent variables that are available experimentally, namely $\langle T\rangle$ and its variance $\langle T^2\rangle$. Note that the (measured) averaged gas refraction index can be identified with $\langle n\rangle$ in the above fluctuation analysis, but the 'true' averaged gas temperature $\langle T\rangle$ should be calculated by using the gas refraction index at the gas average temperature $n(\langle T\rangle)$, both being identical only in non-fluctuating scenarios. Hence, the experimental data should be corrected by subtracting from $\langle n\rangle$ the second term on the right hand-side of (10).

In order to obtain both $\langle T\rangle$ and its variance $\langle T^2\rangle$, a large (~100) sequence of radial gas temperature profiles are obtained from corresponding contrast profiles measured with an exposure time of 1/2000s. As the exposure time is much shorter than that of the current discharge fluctuations (1/100 s), the obtained gas temperature profiles correspond to a nearly constant discharge current phase; i.e., with almost no temperature fluctuations. To account for the small asymmetries in the measured contrast patterns, the measured data for $x<0$ inverted in the point of origin, and the contributions from $x>0$ are averaged and smoothed to decrease the noise level. The Abel inversion (3) is performed on a high-order polynomial curve that fits this profile to reduce the errors to a minimum.

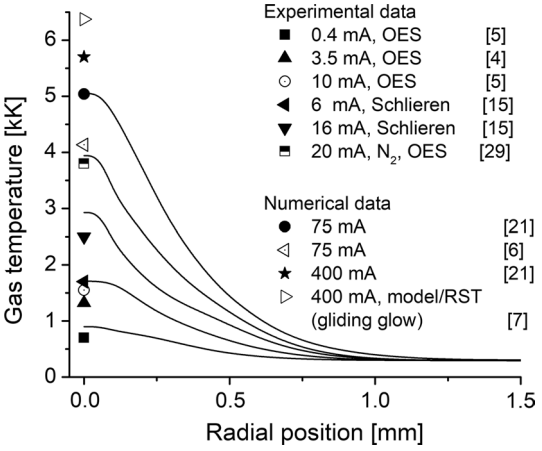

Fig. 8 Selected gas temperature profiles of the discharge obtained from instantaneous data together with relevant available data

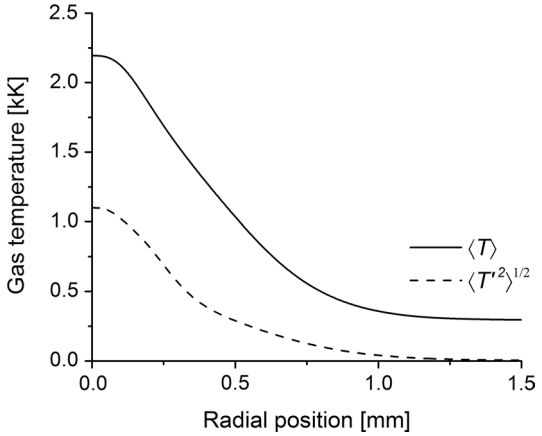

Fig. 9 'True' gas average temperature of the discharge and corresponding 1 level of standard deviation obtained from the analysis of instantaneous data

A number of selected (instantaneous) gas temperature radial profiles together with relevant available data are shown in Fig. 8. Because some errors are unavoidable in the gas temperature calculation if the contrast symmetry assumption is not met (particularly under severe asymmetric conditions), the instantaneous gas temperature profiles obtained do not always appear bell shaped as shown in Fig. 8. However, the time-averaged gas temperature profile (calculated over ~ 100 instantaneous profiles, see Fig. 9) has a well-defined bell shape. It is also observed that the axial values of the derived gas temperature profiles shown in Fig. 8 span a large range from ~ 1000 to 5000 K, thus suggesting that the instantaneous gas temperature nearly follows the evolution of the discharge current. This is expected because the discharge current timescale is much larger than the residence time of gas particles in the discharge column. To show this, consider the timescale for diffusive losses of gas particles from a discharge column of radius R: $t_D \equiv \Lambda_D{}^2/D$, where D is the diffusion coefficient of the neutral particles (which is proportional to $T^{3/2}/p$) and $\Lambda_D \equiv R/2.4$ is the characteristic diffusion length for a cylindrical volume [9]. $D \sim 1 \times 10^{-4}$ m^2/s for air molecules at $T = 1000$ K and R is about 0.5 mm.

Under the conditions considered it follows that t_D is less than or equal to 0.4 ms, much shorter than the discharge current timescale (10 ms).

It should be noted that the found temperature values shown in Fig. 8 agree well with those reported in the literature for atmospheric pressure non-equilibrium discharges [4–7, 15, 21, 29]. The data includes both experimental and numerical gas temperature data for the positive column of discharges with or without tubes and flows (including gliding glows) and different gap lengths; ranging from micro–glow to hybrid discharges. The lowest gas temperature profiles shown in Fig. 8 are consistent with those values ($T = 700$–1550 K) found by OES for air micro-glow discharges at 0.4–10 mA [3–5], while the intermediate gas temperature profiles are consistent with recent schlieren measurements ($T = 1700$–2500 K) for 6–16 mA air micro-glow discharges in a pin-to-pin electrode configuration with a gap length of 2 mm [15]. Axial values are only compared because in convection-stabilized discharges the temperature field at the outer region is sensitive to the gap length [30]. The available experimental data on intermediate-current atmospheric pressure glow (hybrid) discharges in air is scarce. The thermal state of a contracted AC glow discharge with intermediate-current (400 mA) in the flowing atmospheric air (the so-called gliding glow discharge) was investigated by combining RST with numerical simulation [7]. Results indicate a huge gas temperature (e.g., $T = 6373$ K) at the initial state of the discharge. In view of the above-said, it is useful to compare the presented results with the OES data for a pin-to-plate atmospheric pressure contracted glow discharge in nitrogen [29]. A large gas temperature value $T = 3800$ K was obtained for a 20 mA discharge without flow. It should be noted that the temperature of air is typically several hundred Kelvin warmer than nitrogen; probably due to the oxygen, which further facilitate energy transfer to the neutrals and increase the gas temperature [4]. The found gas temperature values also show good agreement with published simulations of intermediate-current atmospheric pressure air discharges [6, 21] (e.g., an axial gas temperature $T = 5000$ K is calculated for a 75 mA discharge in a tube of 1 mm radius [21]). A direct comparison of the obtained results with the numerical data in [21] is possible at the axis of the discharge because thermal conduction is the main mechanism of heat transfer for the central core of the discharge, while convection dominates in the outer region [31].

It is worth to noting that in the Abel inversion of the contrast, values obtained for a specific radial position depend on all the data obtained for radii larger than such a specific position; therefore, deviations (caused by asymmetries of the gas temperature field) may therefore add up towards the axis, thus causing errors in the peak gas temperature values obtained.

The high-gas temperature values shown in Fig. 8 also explain the changes in the dominant ionization mechanism: from ionization by electron-impact at low-currents, to associative ionization in atomic collisions ($O(^3P) + N(^4S, ^2D, ^2P) \rightarrow NO^+ + e$) at high-currents; leading to a negative slope in the voltage–current characteristic of the discharge –as shown in Fig. 1 b)– [6, 21, 32]. It is worth noting that the measured voltage drop suggests that the regime studied is still a glow discharge sustained by secondary emission, however, the inferred high-gas temperature values (as well as the negative voltage–current characteristic) suggests that the charge reproduction in the gap is not provided by direct–electron impact ionization, as in glows; but by thermal ionization, as in arcs. These characteristics indicate that the regime studied can be considered as a hybrid discharge, sharing typical properties of both diffusive glow and thermal arc discharges.

Figure 9 shows the 'true' time-averaged gas temperature value for ~ 100 instantaneous measurements. The level of 1 standard deviation of the same data is also given. Large fluctuations of about 50% of the averaged gas temperature are shown at the axis

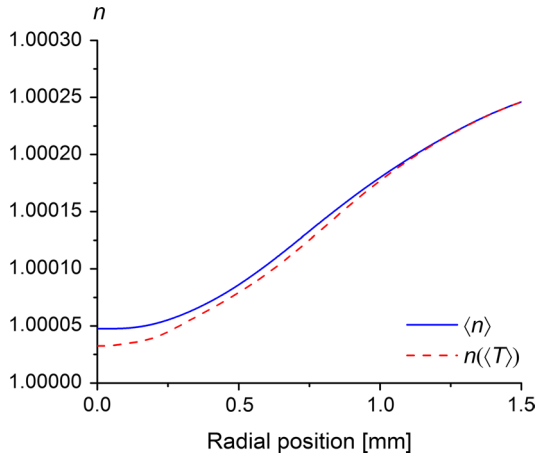

Fig. 10 Average gas refraction index and that corresponding to the gas average temperature

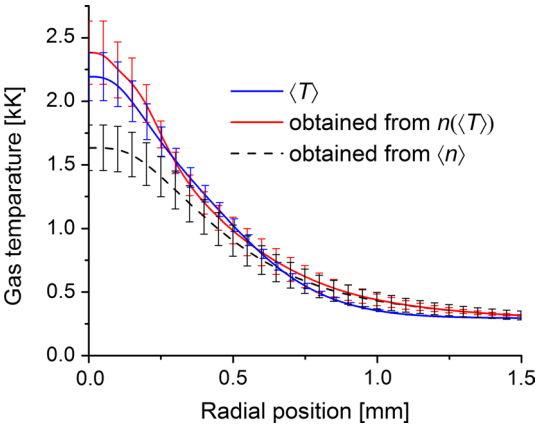

Fig. 11 Gas average temperature profiles obtained from the average gas refraction index $\langle n \rangle$, and that corresponding to the gas average temperature $n(\langle T \rangle)$. For comparative purposes, the 'true' gas average temperature $\langle T \rangle$ is also shown

of the discharge. Figure 10 shows the measured gas refraction index $\langle n \rangle$ profile obtained from averaged data together with the corresponding profile $n(\langle T \rangle)$ calculated from (10) for the average gas temperature $\langle T \rangle$ and variance $\langle T^2 \rangle$ obtained from instantaneous data. To do this, a consistent tenth-order expansion on T' was carried out in the second term on the right hand-side of (10). An appreciable deviation between both profiles is shown close to the discharge axis. This behavior is consistent with the large fluctuations of the gas temperature there. The corresponding gas temperature profiles are shown in Fig. 11. Error bars are mainly associated with some background fluctuations during the measurements, which also affect the calibration process. For comparative purposes, the profile of $\langle T \rangle$ and corresponding standard error are also shown. It is seen that the averaging procedure itself modify the profile of the gas refraction index $\langle n \rangle$, leading to substantial errors (up to ~ 30%) in the determination of the gas averaged temperature profile. Despite the uncertainty in the dependence of T' on time, which affects the calculation of $n(\langle T \rangle)$, the agreement between $\langle T \rangle$ and the gas temperature calculated from $n(\langle T \rangle)$ is good. Regarding to the validity of the simplification of setting the air Gladstone–Dale coefficient at its room temperature value for the calculation of the gas refraction index in non-thermal discharges, the results show that it is not accurate enough for discharge

currents larger than ~ 75 mA. Under the conditions considered, only slight corrections occur for the highest discharge currents.

Conclusions

1. A quantitative schlieren technique applied to a hybrid discharge in atmospheric pressure air operating at current pulses at an amplitude of 75 mA and a duration of 10 ms, applied at a frequency of 100 Hz is reported. Particular attention is paid to chemical reactions that occur with increasing air temperature and that influence the Gladstone–Dale coefficient, and to the effects of gas temperature fluctuations on the measured time-averaged data.
2. Axial values of the derived gas temperature profiles span a large range from ~ 1000 to 5000 K during each single current pulse. The found temperature values agree well with those reported in the literature for atmospheric pressure air discharges, ranging from micro-glow to hybrid discharges.
3. Gas temperature fluctuations are shown to noticeable affects measured data if taken for exposure times larger than that of fluctuations. The link between the average gas refraction index in an oscillating scenario to the gas refraction index at the gas average temperature is found.
4. It was also shown that setting the air Gladstone–Dale coefficient at its room temperature value for the calculation of the gas refraction index of non-thermal air discharges is not accurate enough at discharge currents larger than about 75 mA.

Acknowledgements This work was supported by Universidad Tecnológica Nacional (grants PID 5447 and PID 5418), Agencia Nacional de Promoción Científica y Tecnológica (Grant PICT 2018–00702) and CONICET (PIP 2021–2023 GI). L.P is member of the CONICET. E.C. thanks CONICET for their doctoral fellowships. J.C.C. thanks CONICET for his postdoctoral fellowship.

References

1. Bruggeman PJ, Iza F, Brandenburg R (2017) Plasma Sources Sci Technol 26:123002. https://doi.org/10.1088/1361-6595/aa97af
2. Adamovich I et al (2017) J Phys D Appl Phys 50:323001. https://doi.org/10.1088/1361-6463/aa76f5
3. Machala Z, Janda M, Hensel K, Jedlovsky I, Lestinska L, Foltin V, Martisovits V, Morvova M (2007) J Mol Spectrosc 243(2):194–201. https://doi.org/10.1016/j.jms.2007.03.001
4. Staack D, Farouk B, Gutsol A, Fridman A (2008) Plasma Sources Sci Technol 17:025013. https://doi.org/10.1088/0963-0252/17/2/025013
5. Staack D, Farouk B, Gutsol A, Fridman A (2005) Plasma Sources Sci Technol 14:700–711. https://doi.org/10.1088/0963-0252/14/4/009
6. Prevosto L, Kelly H, Mancinelli B, Chamorro JC, Cejas E (2015) Phys Plasmas 22:023504. https://doi.org/10.1063/1.4907661
7. Kong C, Li Z, Alden M, Ehn A (2020) J Phys D Appl Phys 53:085502. https://doi.org/10.1088/1361-6463/ab586f
8. Giuliani L, Xaubet M, Grondona D, Minotti F, Kelly H (2013) Phys Plasmas 20:063505. https://doi.org/10.1063/1.4812463
9. Raizer Y (1991) Gas discharge physics. Springer, Berlin
10. Adams SF, Caplinger JE, Sommers BS (2015) Plasma Sources Sci Technol 24:025031. https://doi.org/10.1088/0963-0252/24/2/025031
11. Settles GS (2001) Schlieren and Shadowgraph Techniques. Springer, Berlin

12. Traldi E, Boselli M, Simoncelli E, Stancampiano A, Gherardi M, Colombo V, Settles GS (2018) EPJ Tech Instrum 5:4. https://doi.org/10.1140/epjti/s40485-018-0045-1
13. Schmidt-Bleker A, Reuter S, Weltmann KD (2015) J Phys D Appl Phys 48:175202. https://doi.org/10.1088/0022-3727/48/17/175202
14. Schäfer J, Foest R, Reuter S, Kewitz T, Šperka J, Weltmann K-D (2012) Rev Sci Instrum 83:103506. https://doi.org/10.1063/1.4761924
15. Xiong Q, Xu L, Wang X, Xiong L, Huang Q, Chen Q, Wang J, Peng W, Li J (2018) J Phys D Appl Phys 51:095207. https://doi.org/10.1088/1361-6463/aaa882
16. Gambling WA, Edels H (1954) Br J Appl Phys 5:36. https://doi.org/10.1088/0508-3443/5/1/309
17. Zhu Y, Zhang Y, Xiao W, Hu Y, Wang D, Zhao X, Ye X (2016) Optik 127:1471–1473. https://doi.org/10.1016/j.ijleo.2015.11.005
18. Hargather MJ, Settles GS (2012) Opt Lasers Eng 50:8–17. https://doi.org/10.1016/j.optlaseng.2011.05.012
19. Chamorro JC, Prevosto L, Cejas E, Kelly H (2018) IEEE Trans Plasma Sci 47(1):473–482. https://doi.org/10.1109/TPS.2018.2869031
20. Vasilev LA (1971) Schlieren methods. Keter Inc, New York
21. Benilov MS, Naidis GV (2003) J Phys D Appl Phys 36:1834–1841. https://doi.org/10.1088/0022-3727/36/15/314
22. Macheret SO, Rich JW (1993) Chem Phys 174(1):25–43. https://doi.org/10.1016/0301-0104(93)80049-F
23. Machala Z, Marode E, Laux CO, Kruger CH (2004) J Adv Oxid Technol 7:133–137. https://doi.org/10.1515/jaots-2004-0206
24. Alpher RA, White DR (1959) Phys Fluids 2:153–161. https://doi.org/10.1063/1.1705906
25. Levitan YS (1996) IEEE Trans Plasma Sci 24(1):137–142. https://doi.org/10.1109/27.491750
26. Chien YK, Benenson DM (1980) IEEE Trans Plasma Sci 8(4):411–417. https://doi.org/10.1109/TPS.1980.4317349
27. Prevosto L, Kelly H, Mancinelli B (2013) Rev Sci Instrum 84:123506. https://doi.org/10.1063/1.4848916
28. Demetriades A (1964) AIAA J 2:1347–1349. https://doi.org/10.2514/3.2553
29. Akishev Y, Grushin M, Karalnik V, Petryakov A, Trushkin N (2010) J Phys D Appl Phys 43:075202. https://doi.org/10.1088/0022-3727/43/7/075202
30. Naidis GV (2007) Plasma Sources Sci Technol 16:297–303. https://doi.org/10.1088/0963-0252/16/2/012
31. Pellerin S, Richard F, Chapelle J, Cormier JM, Musiol K (2000) J Phys D Appl Phys 33:2407. https://doi.org/10.1088/0022-3727/33/19/311
32. Cejas E, Mancinelli B, Prevosto L (2020) Plasma 3(1):12–26. https://doi.org/10.3390/plasma3010003